High-Q impurity photon states bounded by a photonic band pseudogap in an optically thick photonic crystal slab

Se-Heon Kim,[1,2,*] Andrew Homyk,[2,3] Sameer Walavalkar,[2,3] and Axel Scherer[1,2,3]
[1]*Department of Physics, California Institute of Technology, Pasadena, California 91125, USA*
[2]*Kavli Nanoscience Institute, California Institute of Technology, Pasadena, California 91125, USA*
[3]*Department of Electrical Engineering, California Institute of Technology, Pasadena, California 91125, USA*
(Received 6 September 2012; revised manuscript received 28 November 2012; published 14 December 2012)

We show that, taking a two-dimensional photonic crystal slab system as an example, surprisingly high quality factors (Q) over 10^5 are achievable, even in the *absence* of a rigorous photonic band gap. We find that the density of in-plane Bloch modes can be controlled by creating additional photon feedback from a finite-size photonic-crystal boundary that serves as a *low*-Q resonator. This mechanism enables significant reduction in the coupling strength between the bound state and the extended Bloch modes by more than a factor of 40.

DOI: 10.1103/PhysRevB.86.245114 PACS number(s): 42.70.Qs, 42.50.Pq, 42.60.Da

I. INTRODUCTION

Significant reduction in the radiation rate of a pointlike emitter can be achieved by setting up mirrors around it,[1] or by employing photonic crystals (PhCs),[2,3] which is a photonic analog of atomic crystals for electron waves.[4] It has long been believed that the existence of the photonic band gap (PBG) is essential to achieving a *spatially localized* high-Q electromagnetic bound state using a PhC cavity. Thus, most efforts so far have focused on artificial dielectric structures possessing a PBG.[5–8] Donor- or acceptorlike impurity photon states can be formed at the location of a crystal defect.[9] Such a localized state (with small mode volume V) has drawn much attention in the context of cavity quantum electrodynamics (cQED) experiments[10,11] where the use of high Q/V cavities is essential to enhancing light-matter interaction.

Due to fabrication related difficulties, three-dimensional (3D) PhCs have been replaced with a lower dimensional counterpart relying on index guiding in one or two dimensions. Often, this assumes the form of a thin dielectric slab,[12] whose thickness (T) is roughly equal to half the effective wavelength ($T \approx \lambda/2n_{\text{eff}}$) in order to optimize the size of the in-plane PBG. One representation of such a design is shown in Figs. 1(a) and 1(b). Note that a 2D PhC with the triangular lattice of air holes supports the PBG only for *even* guided modes, where the symmetry is defined with respect to the mirror plane at $z = 0$. However, this *incomplete* PBG does not preclude the possibility of high-Q defect states, because the same mirror symmetry ensures that the defect mode with the *even* symmetry will be *completely* decoupled from all *odd* guided modes. Lowering the dimensionality often creates new symmetries that can be exploited, making the condition for localized photon states less stringent.

It is well established that an optically-*thick* PhC slab does not support any PBG for both *even* and *odd* symmetries.[12,13] As an example, in Fig. 1(d), we present a photonic band structure (ω-k diagram) for *even* Bloch modes in a *thick* PhC slab with $T = 1.731a$. The formation of the PBG is hindered by the higher-order slab modes lying between the 1st and the 5th bands. Note that the energy gap defined by the 1st and the 5th bands ($\triangle\omega_{1-5}$) will remain more or less constant as T increases and, in the limit of $T \to \infty$, $\triangle\omega_{1-5}$ will approach the PBG of an ideal 2D PhC.[12] Also note that, though all bands, $\mathbf{E}_{(\text{Bloch})}(\mathbf{r})$, shown in Fig. 1(d) are mutually orthogonal, the bound state in a defect region, $\mathbf{E}_{(\text{cav})}(\mathbf{r})$, in general, *can* couple to any of the higher-order Bloch modes. However, this coupling strength, $|\kappa_{c,B}| \sim |\int d^3\mathbf{r}\triangle\epsilon\mathbf{E}_{(\text{cav})} \cdot \mathbf{E}^*_{(\text{Bloch})}|$,[14] shouldn't be strong, because $\mathbf{E}_{(\text{cav})}(z)$ resembles $\mathbf{E}_{(\text{Bloch})}(z)$ of the 1st band. In this sense, any optically-thick PhC slab bears a *pseudo*-PBG. A similar pseudo-energy gap in solid state physics can create *resonance* states.[15] Here, the photonic counterpart can be easily manipulated with high precision by means of the mature modern nanofabrication technology.

In this paper, we will show how $\kappa_{c,B}$ can be controlled by setting up simple mirror boundaries around the finite size PhC resonator [see Figs. 1(a) and 5(e)]. The additional boundary conditions imposed by the mirrors can alter the density of Bloch states in the momentum space (**k** space). Thus, in relation to the **k** spectrum of $\mathbf{E}_{(\text{cav})}$,[16] $\kappa_{c,B}$ can experience significant change. We note that the situation is analogous to the well-known cQED example of a point dipole source ($\approx$ the hexapole mode) in an optical resonator ($\approx$ the low-Q resonator defined by the boundary termination).[17]

The paper is organized as follows: In Sec. II, we begin with the simplest boundary condition—air, which may appear impractical due to its air-suspended nature. However, we intentionally choose this moderately reflecting boundary in order to emphasize that $\kappa_{c,B}$ plays the more important role in the Q optimization than the reflectivity itself. In Sec. III, we discuss the case of a metal boundary condition. We show one feasible design for a current-injection PhC laser based on this metal-bridge structure. We also discuss other potential candidates for practical devices based on the 2D PhC.

II. BOUNDARY TERMINATION BY AIR

A. 3D numerical simulation

We perform fully-vectorial 3D numerical simulations using the finite-difference time-domain method (FDTD) to understand the mutual interaction between $\mathbf{E}_{(\text{cav})}$ and $\mathbf{E}_{(\text{Bloch})}$. First, we study the energy decay rate (γ) of the hexapole mode[18] shown in Fig. 1(b). The total decay rate (γ_{tot}) can be decomposed into the decay rates into the horizontal direction (γ_{horz}) and the out-of-plane direction (γ_{vert}). Then, γ is translated into Q factor through $Q \equiv \omega/\gamma$. Thus,

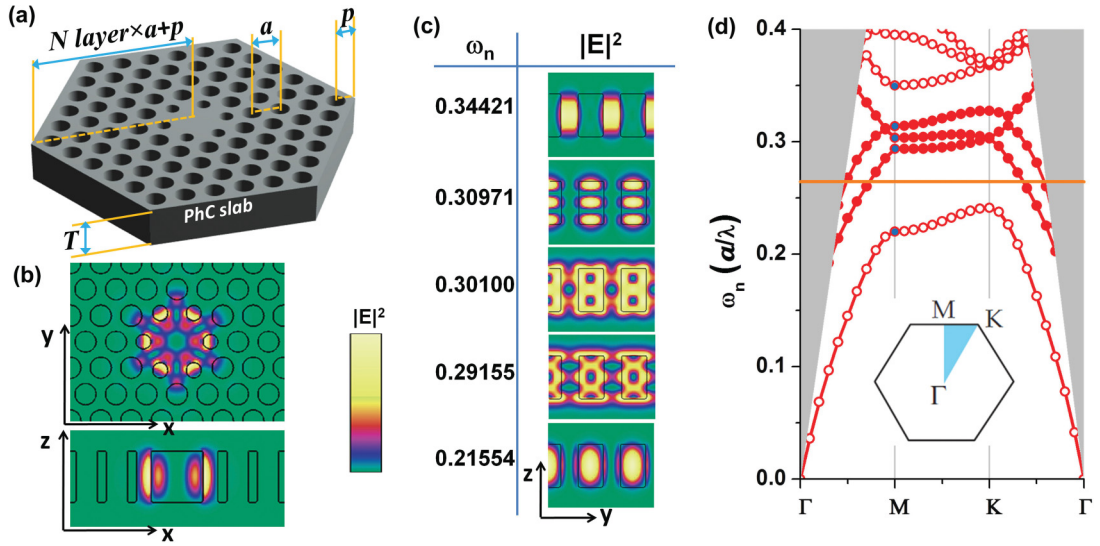

FIG. 1. (Color online) (a) A 3D rendering of the photonic crystal cavity to be studied in this paper. The number of photonic crystal hole layers (*N layer*) and the boundary termination (p) are to be varied. a is the lattice constant of the 2D triangular-lattice photonic crystal with the background air holes, R, of $0.35a$. The refractive index of the slab is assumed to be 3.4. The six nearest neighbor holes are reduced ($Rm = 0.25a$) and slightly pushed away (by a scale factor of 1.1) from the defect center. (b) $|\mathbf{E}|^2$ distribution of the hexapole mode in a $T = 1.731a$ slab. (c) Cross-sectional views of the first five lowest Bloch modes at M point. These modes all have even symmetries with respect to the plane at $z = 0$. (d) The photonic band structure for all even Bloch modes. The hexapole mode resonance shown in (b) ($\omega_n \sim 0.265$) is represented by the horizontal line, in which ω_n is the normalized frequency defined by $\omega_n \equiv a/\lambda$.

$1/Q_{\text{tot}} = 1/Q_{\text{horz}} + 1/Q_{\text{vert}}$.[13] Note that we set up detection planes for the Poynting energy flux ($\sim\mathbf{E} \times \mathbf{H}^*$) away from the mirror boundary, so that γ_{horz} accounts for the reflection/transmission at the PhC-air discontinuity.

In Fig. 2, we consider the two boundary terminations of $p = \infty$ and $p = 1.2a$. For $p = \infty$, Q_{tot} tends to be saturated by Q_{horz}; Q_{tot} approaches $44\,000 \sim 48\,000$ as N layer > 8.[13] In fact, this particular choice of the boundary termination $p = \infty$ approximately ensures negligibly small reflection off the interface. Alternatively, we can simulate the transparent boundary condition by overlapping the perfectly matched layer

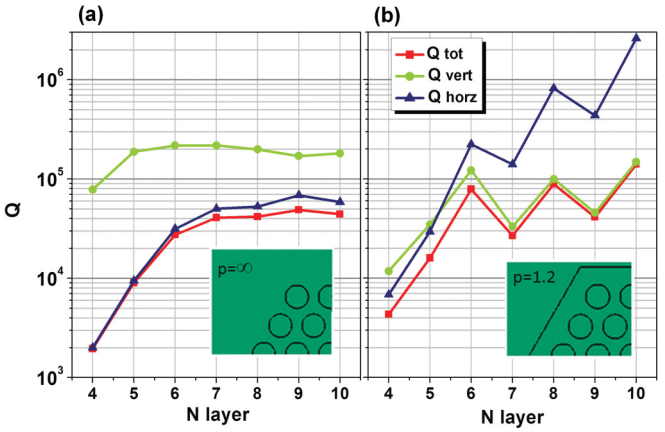

FIG. 2. (Color online) Q_{tot}, Q_{vert}, and Q_{horz} of the hexapole mode for two different boundary terminations, (a) $p = \infty$ and (b) $p = 1.2a$. When the mirror boundary effect is *weak* ($p = \infty$), Q_{horz} is limited by about 60 000 due to the coupling to the in-plane Bloch modes. However, in the case of the abrupt termination by air, Q_{horz} can be made over 2 600 000.

in the FDTD with the PhC air holes,[19] which results in the similar saturated Q_{horz} of $\sim$60 000 ($\equiv Q_{\text{horz}}^{(\text{sat})}$).

Usually, the reflection coefficient at the PhC air boundary is not so large as $0.5 \sim 0.6$.[20] However, drastically different behaviors can be seen by forming simple mirrors with $p = 1.2a$ [Fig. 2(b)]. (i) All Q values *strongly* modulate with N *layer*. (ii) Q_{horz} can be brought up to a surprisingly high value of $\sim 2.6 \times 10^6$ at N *layer* $= 10$. This implies that γ_{horz} can be reduced by more than a factor of 40 compared with the case of minimal reflection ($p = \infty$). (iii) Since $Q_{\text{horz}} \gg Q_{\text{vert}}$, now the hexapole mode emits more photons into the out-of-plane direction. Interestingly, all Qs modulate in the same fashion; whenever Q_{horz} is peaked, so is Q_{vert}. Therefore, the abrupt boundary termination does not simply redirect the in-plane guided energy into the out-of-plane radiation. Rather, there should be a common physical principle for the observed enhancement and suppression. Moreover, note that the maximum Q_{tot} of 1.4×10^5 in the present case can be further increased by employing a higher Q_{vert} cavity mode. Also note that Q_{vert} of the hexapole mode is slightly lowered by the use of finite space grids ($\triangle = a/20$) used in the FDTD simulation.[21]

More detailed analyses are performed as we finely tune the mirror boundary conditions. Specifically, we tune p in the range of 0.8–1.2a as a means to control the phase shift (ϕ) upon reflection. Here, we will provide direct *graphical* evidence for the enhancement/suppression of the in-plane Bloch modes. In order to visualize the very weak near fields in the outskirt regions, we adopt the saturated color scheme in which 1/1000 of the intensity maximum is taken as the upper bound. In Figs. 3(a)–3(c), we present $|\mathbf{E}(\mathbf{r}_{||}, z = 0)|^2$ of the hexapole mode for three different $p = 0.8$, 1.0, and $1.2a$. We take only one-sixth area (cut by the two Γ-K lines) of the hexapole mode

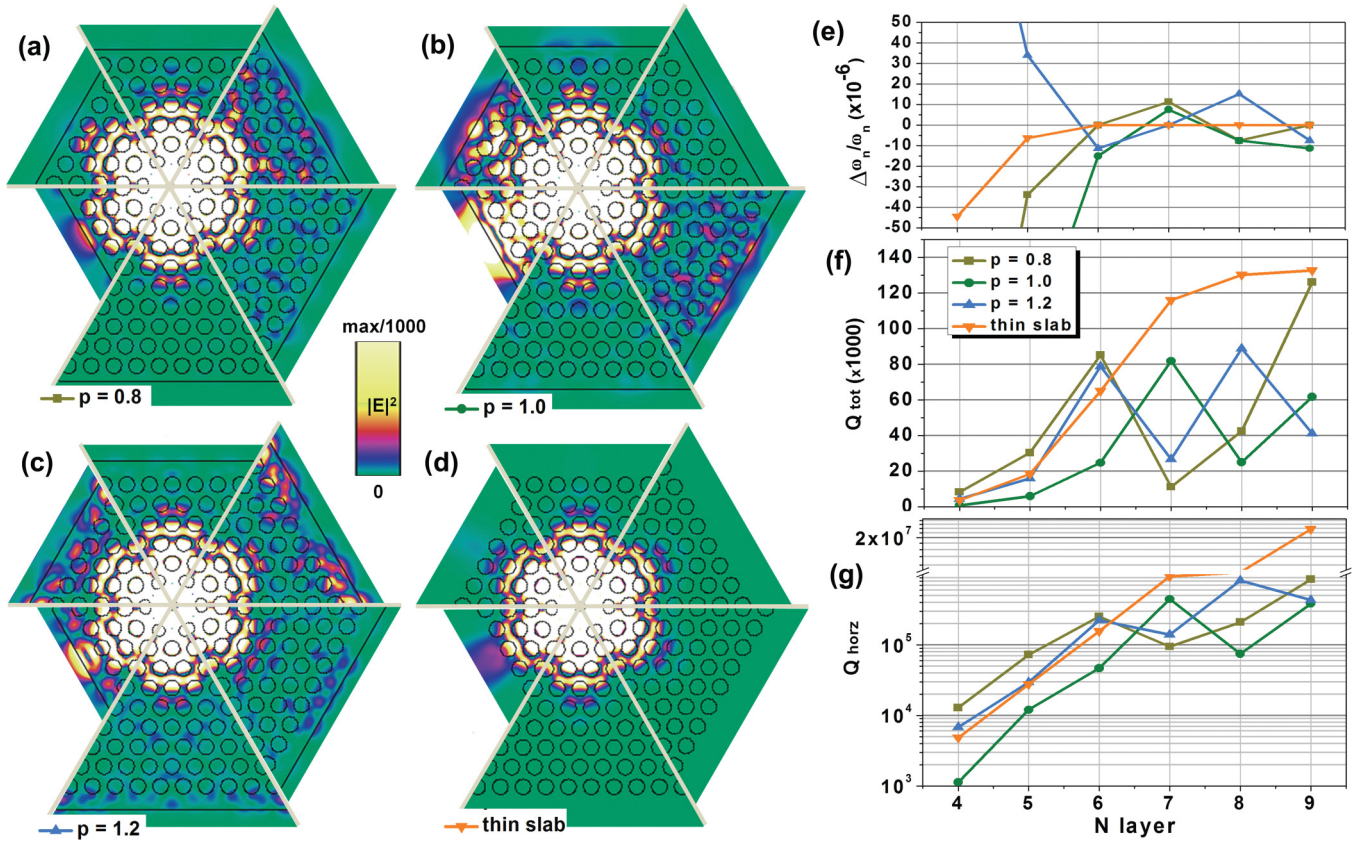

FIG. 3. (Color online) (a)–(c) Top-down views ($|\mathbf{E}|^2$) of the hexapole resonances in a $T = 1.731a$ slab as we increase N *layer* from 4 to 9 (in the clockwise direction) for three different boundary terminations of $p = 0.8, 1.0$, and $1.2a$, respectively. (d) The hexapole resonances in a *thin* ($T = 0.488a$) slab for $p = \infty$ are presented in the same manner used in (a)–(c). Note that this thin slab possesses the in-plane photonic band gap. (e) Q_{horz} and (f) Q_{tot} for the hexapole resonances shown in (a)–(d).

profile for each N *layer*, then combine with plots of different N *layer*s to create one image filling up to 360°. We also provide a similar plot for a PBG-confined hexapole mode in Fig. 3(d), corresponding to a slab thickness of $0.488a$. For quantitative analyses, we also provide graphs for Q_{tot} [Fig. 3(f)] and Q_{horz} [Fig. 3(g)] as well as the resonance frequency shift $\triangle\omega_n/\omega_n$ [Fig. 3(e)].

We find that, at (N *layer*, p) = (9, $0.8a$), $|\mathbf{E}_{(\text{Bloch})}(\mathbf{r}_{||})|^2$ is *almost completely suppressed*, which is comparable with that of the PBG-confined case shown in Fig. 3(d). On the other hand, at certain combinations of (N *layer*, p), $|\mathbf{E}_{(\text{Bloch})}(\mathbf{r}_{||})|^2$ becomes quite strongly pronounced; for example, see (7, $0.8a$), (8, $1.0a$), and (7, $1.2a$). For small N *layer* such as at (N *layer* $\leqslant 5$, $p = 1.0a$), it seems natural to have more intense photon tunneling than the equivalent PBG-confined case. However, by *slightly* tuning p, the strong in-plane loss in the previous case can be greatly reduced by more than a factor of 10, whose resultant Q_{tot} and Q_{horz} can be higher than those of the PBG-confined case.[22] This result may find a practical importance in applications where a device miniaturization is required while keeping Q reasonably high.

We find that $|\mathbf{E}_{(\text{Bloch})}(\mathbf{r}_{||})|^2$ variations can explain peaks and dips observed in Q_{horz} or Q_{tot}. We also note that the more intensified $|\mathbf{E}_{(\text{Bloch})}(\mathbf{r}_{||})|^2$ in the outskirt region can contribute to the excessive scattering losses into the vertical direction, thereby lowering Q_{vert}. In short, what we have shown here is that $\kappa_{c,B}$ strongly depends on the detailed boundary conditions. $\kappa_{c,B}$ obviously depends on the size of the hexagonal boundary, which determines the phase thickness of the 2D cavity. It is also understandable that p is a very critical parameter controlling the density of in-plane Bloch modes, as has been seen in many cQED examples of an atom and a cavity. Further evidence of this analogy can be found in Fig. 3(e), which reports the fractional frequency shift. Even using sufficiently thick PhC mirrors with N *layer* $\geqslant 6$, the thick-slab cases show noticeable modulations in $\triangle\omega_n/\omega_n$ order of $\pm 10^{-5}$, while the PBG-confined case does not. These energy-level shifts[17] are signatures of the coupling between $\mathbf{E}_{(\text{cav})}(\mathbf{r})$ and $\mathbf{E}_{(\text{Bloch})}(\mathbf{r})$ and can be explained in terms of $\kappa_{c,B}$.[14]

B. Coupled-mode theory

Though the FDTD provides very accurate first-principle means to understand the $\kappa_{c,B}$ modulation, we have not been quite convinced as to how the simple boundary termination (hence the *low* Q) can enable such large modulations in Q_{horz} (and Q_{tot} as well). Therefore, it would be instructive to develop a simple model in the spirit of the coupled mode theory (CMT).[14,23] To begin, we would like to note that the in-plane hexapole mode profile, $|\mathbf{E}_{(\text{cav})}(\mathbf{r}_{||})|^2$, can be approximated in terms of the three M-point wavevectors of $\mathbf{k}_{M1} = (0,1)|\mathbf{k}_M|$, $\mathbf{k}_{M2} = (\sqrt{3}/2, 1/2)|\mathbf{k}_M|$, and $\mathbf{k}_{M3} = (\sqrt{3}/2, -1/2)|\mathbf{k}_M|$ with

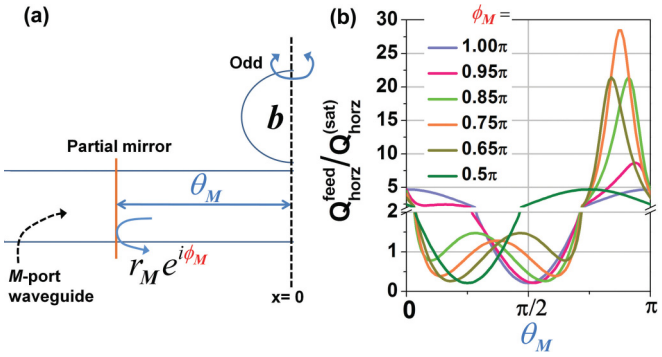

FIG. 4. (Color online) (a) In our coupled-mode model, the hexapole mode is assumed to couple only to the Γ-M wavevectors. For further simplification, the solution for the entire system is *projected* into the x direction. The hexapole symmetry ensures the odd mirror symmetry with respect to the $x = 0$ plane. (b) Q_{horz} enhancement factors in Eq. (4). All plots assume $r_M = 0.6$.

$|\mathbf{k}_M| = 2\pi/\sqrt{3}a$. For example, $|\mathbf{E}_{(\text{cav})}(\mathbf{r}_{||})|^2 \approx |\sin(\alpha\mathbf{k}_{M1}\cdot\mathbf{r}_{||}) - \sin(\alpha\mathbf{k}_{M2}\cdot\mathbf{r}_{||}) - \sin(\alpha\mathbf{k}_{M3}\cdot\mathbf{r}_{||})|^2$ with a correction factor $\alpha > 1$.[24] For our hexapole mode, α is ~1.1 based on the $\mathbf{k}$-space intensity distribution, $|\tilde{\mathbf{E}}_{(\text{cav})}(\mathbf{k})|^2$.[21] This is the reason the outskirt region of the hexapole mode resembles the M-point Bloch modes.[25]

To simplify our CMT model, we assume that the hexapole mode couples *only* to the six M-point wavevectors, $\beta\times(\mathbf{k}_{M1}, \mathbf{k}_{M2}, \mathbf{k}_{M3}, -\mathbf{k}_{M1}, -\mathbf{k}_{M2}, -\mathbf{k}_{M3})$, where β is a scale factor ~ 0.7 as evidenced from the photonic band structure in Fig. 1(d). Now we emphasize that these M-point wavevectors ($\{\beta\mathbf{k}_M\}$) are *closed* upon reflections at the six hexagonal facets. Thus, we may consider the whole set of wavevectors, $\{\beta\mathbf{k}_M\}$, as a *channel* or a *port* in the CMT formulation [Fig. 4(a)]. Under these assumptions, our hexapole mode can be viewed as *side-coupled* to the port.[26] Then, the time evolution of the hexapole mode's energy amplitude (b) can be described by

$$\frac{db}{dt} = \left[i\omega_0 - \frac{\gamma_{\text{vert}} + \gamma_{\text{horz}}}{2}\right]b + \kappa_M S_{+M}, \tag{1}$$

where the last term describes the *total incoming* power as a result of the feedback by the boundary termination. We assume that S_{+M} is measured at the *inner* boundary of the partial mirror shown in Fig. 4(a) and consists of the Bloch waves with $\{\beta\mathbf{k}_M\}$. The CMT states that κ_M cannot be arbitrarily determined but rather it should be connected by the decay rate into the waveguide port such that $\kappa_M = \sqrt{2\gamma_{\text{horz}}}e^{-i\theta_M}$.

When the effect of the photon feedback is weak as in the case of $p = \infty$, we can set $S_{+M} = 0$ in Eq. (1). Then, $|b|^2$ decays exponentially with $\gamma_{\text{horz}} = |\kappa_M|^2/2 = \omega_0/Q_{\text{horz}}^{(\text{sat})}$. However, when there is a feedback mechanism, γ_{horz} is not a constant but varies with θ_M and ϕ_M (reflection phase). For this general situation, we need an additional set of equations, which can be derived from the CMT.[27] For example, the outgoing power (S_{-M}) and the incoming power (S_{+M}) are related to each other by b through

$$S_{-M} = e^{-2i\theta_M}S_{+M} + \sqrt{2\gamma_{\text{horz}}}e^{-i\theta_M}b. \tag{2}$$

We define the scattering matrix of the partial mirror such that $S_{+M} = r_M e^{i\phi_M}S_{-M}$. Then, the modified Q_{horz} ($\equiv Q_{\text{horz}}^{\text{feed}}$) can be written using the definition of Q ($\equiv\omega\times$ [total energy stored in the resonator]/[total power loss into the port]),

$$Q_{\text{horz}}^{\text{feed}} = \omega^{\text{feed}}\frac{|b|^2}{t_M^2|S_{-M}|^2}. \tag{3}$$

In general, ω^{feed} (the resonance frequency in the presence of the feedback) differs from the original ω_0 as we have seen from the FDTD result in Fig. 3(e). However, we can assume $\omega^{\text{feed}} \approx \omega_0$ since the fractional change in ω is much less than 1%. Note that the partial mirror is assumed to be lossless such that $r_M^2 + t_M^2 = 1$. After solving S_{-M} and S_{+M} for b, we obtain the expression for the Q_{horz} enhancement, $Q_{\text{horz}}^{\text{feed}}/Q_{\text{horz}}^{(\text{sat})}$ ($=\gamma_{\text{horz}}/\gamma_{\text{horz}}^{\text{feed}}$),

$$\frac{Q_{\text{horz}}^{\text{feed}}}{Q_{\text{horz}}^{(\text{sat})}} = \frac{1 + r_M^4 - 2r_M^2\cos(2\phi_M + 4\theta_M)}{(1 - r_M^2)\left[1 + r_M^2 + 2r_M\cos(\phi_M - 2\theta_M)\right]}. \tag{4}$$

Figure 4(b) shows plots of Eq. (4) for several ϕ_M values, while r_M is fixed at 0.6. The model also expects drastic modulations in Q_{horz} depending on where we locate the resonator with respect to the $|\mathbf{E}|^2$ envelop of the low-Q Fabry-Perot type resonator. For example, when $\phi_M = 1.0\pi$, Q_{horz} enhancement is maximized to be about 5 at $\theta_M = \pi$ (= effective half wavelength), which can be understood considering that $|\mathbf{E}|^2 = 0$ at $x = 0$. Interestingly, tuning ϕ_M slightly can greatly improve the enhancement; $\phi_M = 0.75\pi$ results in the maximum $Q_{\text{horz}}^{\text{feed}}/Q_{\text{horz}}^{(\text{sat})}$ very close to 30. We also find that the ϕ_M tuning inevitably alters the optimal θ_M for Q, which agrees with the FDTD results in Fig. 3; the small tuning in p changes the optimal N *layer* for Q.

It should be noted that we have assumed only one $\mathbf{k}$ port and such a large enhancement holds true only for that port. However, if the defect state could excite many in-plane Bloch waves with different wavevectors thereby creating many $\mathbf{k}$ ports, the overall Q_{horz} enhancement contributed from different $\mathbf{k}$ ports will be averaged out to be 1 as Eq. (4) expects. For example, multiple $\mathbf{k}$ ports might be involved if T were too thick (since this would allow more higher-order slab modes with many $\mathbf{k}$s) or if the boundary termination would not retain the hexapole symmetry (since $\mathbf{k}_M$ cannot be conserved upon reflections).

III. BOUNDARY TERMINATION BY METAL

We now discuss the case of a highly-reflective ($r_M \approx 1$) mirror boundary condition—metal, as depicted in Fig. 5(e). We note that such a structure is experimentally realizable.[30,31] We investigate the same hexapole resonance shown in Fig. 1(b) except for the boundary condition. In this case, Q_{horz} is a meaningless quantity because a sufficiently-thick metal layer (thicker than the optical skin depth, which is usually <30 nm at λ = 1300 nm)[22] can completely block the light transmission. Also note that a small fraction of the incident energy, typically about 1~2%, can be absorbed upon a single reflection. Therefore, most of the photon energy leaks into the out-of-plane direction and $Q_{\text{tot}} \approx Q_{\text{vert}}$ for the entire tuning range of the parameters.

In Figs. 5(a) and 5(b), we calculate Q_{tot} as we vary N *layer* and p. As expected, we observe strong modulations in Q_{tot}

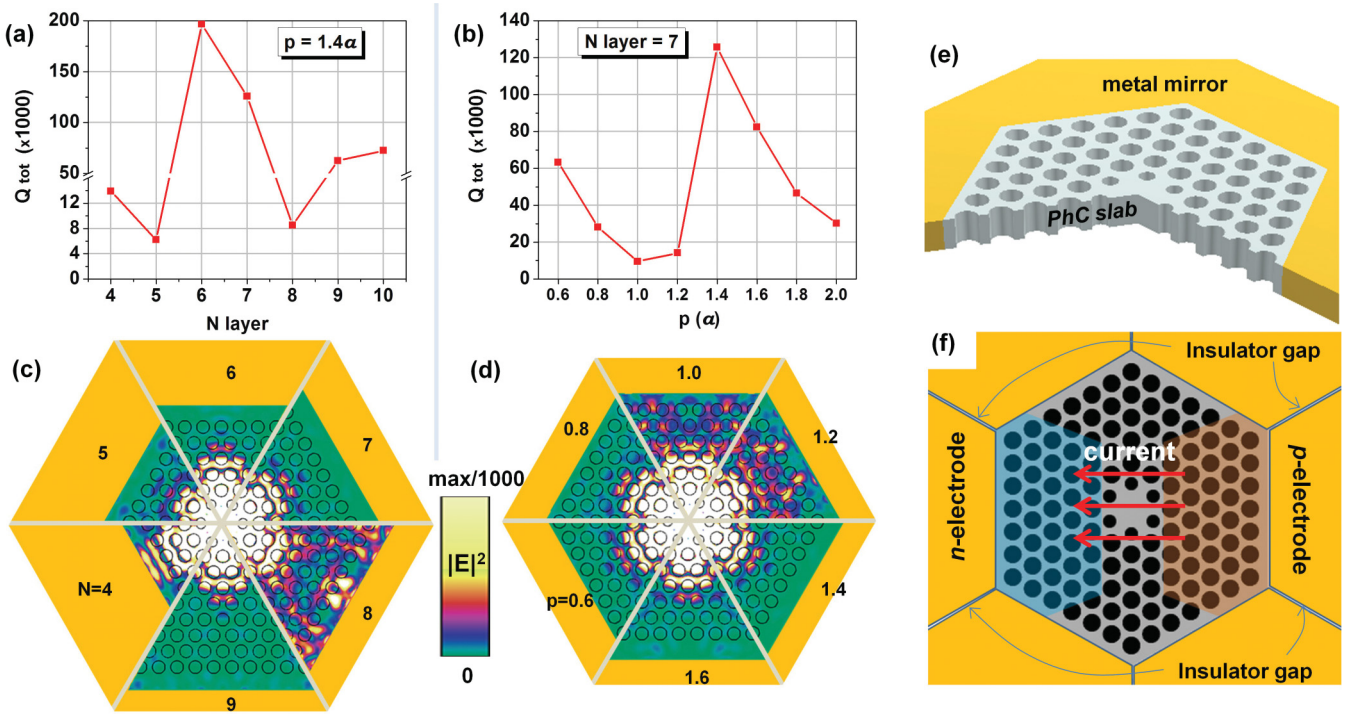

FIG. 5. (Color online) The air boundary condition is now replaced with a metal slab. The metal is assumed as gold, which is modeled as a single-pole Drude medium (Ref. 28). We calculate Q_{tot} [(a) and (b)] and $|\mathbf{E}(\mathbf{r}_{||}, z = 0)|^2$ [(c) and (d)] as we vary *N layer* (while p is fixed to $1.4a$) and p (while *N layer* is fixed to 7) for the photonic crystal slab ($T = 1.731a$) shown in (e). (f) A schematic diagram shows how the metal reflector on the side can be designed to function as a current injection electrode. The conical area shaded in red (blue) denotes a p-doped (an n-doped) region by using ion implantation, forming a laterally p-i-n doped structure (Ref. 29).

(or Q_{vert}) either by *N layer* or p. The maximum Q_{tot} is found to be very close to 2.0×10^5, which is about a 40% increase compared with the air boundary case. It should be noted that the Q_{tot} modulation here is not so much enhanced compared with the case of the *low*-reflectivity air/dielectric boundary.

Though the CMT model in Sec. II B is used to explain Q_{horz} variation, the essentially same view on the coupling strength ($\kappa_{c,B}$) modulation can also be employed in the present case. As we have seen in Sec. II A, Q_{tot} and Q_{horz} tend to modulate in the same fashion [see Figs. 3(f) and 3(g)]. Therefore, the Q_{tot} modulation observed here should have the same origin as in Sec. II. Figs. 5(c) and 5(d) confirm the aforementioned conjecture. We plot $|\mathbf{E}(\mathbf{r}_{||})|^2$ using the same saturated color scheme as used in Figs. 3(a)–3(d). Again, we can verify that the parameter combination giving *low* Q_{tot} corresponds to the *strongly* intensified $|\mathbf{E}_{(\text{Bloch})}(\mathbf{r}_{||})|^2$.

Since the high-Q condition does not critically depend on the use of high r_M, instead of having metal contacts on the six hexagonal facets, evaporated metal films on the top surface of the PhC slab may function quite well as partial mirrors. If this is the case, we can envisage a number of unconventional functionalities integrated into a single component of the metal contact, for example, as a side reflector and/or an optical antenna.[32] With all these possibilities in mind, in Fig. 5(f) we present one exemplary design showing how the surrounding metal reflector discussed in this section can be adopted as an electrical contract for current injection PhC nanolasers. As for the PhC slab, we assume the laterally doped p-i-n structure proposed very recently.[29]

There still remain other practical forms of the 2D PhC resonator: A low index cladding material can be placed underneath as a supporting structure. An optically-*thick* PhC slab can be placed on a metal substrate, which is another practical form of the current injection PhC nanolaser.[28]

IV. SUMMARY

In summary, we study a quasibound photon state within a PhC that does not possess a rigorous PBG. We show that the density of in-plane Bloch modes can be controlled by the termination of the finite-size PhC. The coupling strength between the bound state and the extended Bloch modes can be reduced by more than a factor of 40 in the case of a thick PhC slab. By removing the thickness constraint of $T \approx \lambda/2n_{\text{eff}}$, many unconventional cavity designs which were previously discarded because they cannot support a PBG can now be reconsidered. Though the present study merely focuses on a 2D PhC system, the same principle can be applied to the design of a high-Q defect mode in the 3D PhC lacking a full 3D PBG.[33]

ACKNOWLEDGMENTS

This work was supported by the Defense Advanced Research Projects Agency under the Nanoscale Architecture for Coherent Hyperoptical Sources program (W911NF-07-1-0277) and by the National Science Foundation under NSF CIAN ERC (EEC-0812072). A.H. appreciates the generous support of the ARCS Foundation.

*seheon@caltech.edu

[1] E. M. Purcell, Phys. Rev. **69**, 681 (1946).

[2] E. Yablonovitch, Phys. Rev. Lett. **58**, 2059 (1987).

[3] S. John, Phys. Rev. Lett. **58**, 2486 (1987).

[4] J. D. Joannopoulos, S. G. Johnson, J. N. Winn, and R. D. Meade, *Photonic Crystals: Molding the Flow of Light*, 2nd ed. (Princeton University Press, Princeton, NJ, 2008).

[5] E. Yablonovitch, J. Opt. Soc. Am. B **10**, 283 (1993).

[6] S. Noda, K. Tomoda, N. Yamamoto, and A. Chutinan, Science **289**, 604 (2000).

[7] E. Chow, S. Lin, S. Johnson, P. Villeneuve, J. Joannopoulos, J. Wendt, G. Vawter, W. Zubrzycki, H. Hou, and A. Alleman, Nature (London) **407**, 983 (2000).

[8] M. Maldovan and E. L. Thomas, Nat. Mater. **3**, 593 (2004).

[9] E. Yablonovitch, T. J. Gmitter, R. D. Meade, A. M. Rappe, K. D. Brommer, and J. D. Joannopoulos, Phys. Rev. Lett. **67**, 3380 (1991).

[10] T. Yoshie, A. Scherer, J. Hendrickson, G. Khitrova, H. M. Gibbs, G. Rupper, C. Ell, O. B. Shchekin, and D. G. Deppe, Nature (London) **432**, 200 (2004).

[11] S. Noda, M. Fujita, and T. Asano, Nat. Photon. **1**, 449 (2007).

[12] S. G. Johnson, S. Fan, P. R. Villeneuve, J. D. Joannopoulos, and L. A. Kolodziejski, Phys. Rev. B **60**, 5751 (1999).

[13] S.-H. Kim, J. Huang, and A. Scherer, Opt. Lett. **37**, 488 (2012).

[14] H. A. Haus, *Waves and Fields in Optoelectronics* (Prentice-Hall, Englewood Cliffs, NJ, 1984).

[15] O. Madelung, *Introduction to Solid-State Theory* (Springer-Verlag, Berlin, 1978), Chap. 14.

[16] K. Srinivasan and O. Painter, Opt. Express **10**, 670 (2002).

[17] E. A. Hinds, in *Cavity Quantum Electrodynamics*, edited by P. R. Berman (Academic Press, Inc, Orlando, 1994).

[18] H.-Y. Ryu, M. Notomi, and Y.-H. Lee, Appl. Phys. Lett. **83**, 4294 (2003).

[19] M. Koshiba, Y. Tsuji, and S. Sasaki, Microwave and Wireless Components Letters, IEEE **11**, 152 (2001).

[20] E. Istrate, A. A. Green, and E. H. Sargent, Phys. Rev. B **71**, 195122 (2005).

[21] S.-H. Kim, S.-K. Kim, and Y.-H. Lee, Phys. Rev. B **73**, 235117 (2006).

[22] For the thin PhC slab, we find that $p \sim 1.0a$ causes excessive scattering losses at the termination boundaries, resulting in lower Q than the $p = \infty$ case. For fair comparisons between *thin* and *thick* slabs, we assume both modes oscillate at approximately the same resonant wavelength of 1300 nm, which can be achieved by choosing a of the thin slab and the thick slab to be 410 nm and 350 nm, respectively.

[23] S. Fan, W. Suh, and J. D. Joannopoulos, J. Opt. Soc. Am. A **20**, 569 (2003).

[24] O. Painter and K. Srinivasan, Phys. Rev. B **68**, 035110 (2003).

[25] G.-H. Kim, Y.-H. Lee, A. Shinya, and M. Notomi, Opt. Express **12**, 6624 (2004).

[26] The side-coupling configuration may describe the situation better than the butt-coupling, because (i) the pointlike defect structure occupies only a small fraction of the entire 2D cavity and (ii) the 2D Bloch waves rather *freely* move from the left side to the right side without being assisted by the resonance of the defect.

[27] C. Manolatou, M. J. Khan, S. Fan, P. R. Villeneuve, H. A. Haus, and J. D. Joannopoulos, IEEE J. Quantum Electron. **35**, 1322 (1999).

[28] S.-H. Kim, J. Huang, and A. Scherer, J. Opt. Soc. Am. B **29**, 577 (2012).

[29] B. Ellis, M. A. Mayer, G. Shambat, T. Sarmiento, J. Harris, E. E. Haller, and J. Vuckovic, Nat. Photon. **5**, 297 (2011).

[30] S. Zamek, L. Feng, M. Khajavikhan, D. T. H. Tan, M. Ayache, and Y. Fainman, Opt. Express **19**, 2417 (2011).

[31] J. Huang, S.-H. Kim, and A. Scherer, Opt. Express **18**, 19581 (2010).

[32] E. R. Brown, C. D. Parker, and E. Yablonovitch, J. Opt. Soc. Am. B **10**, 404 (1993).

[33] M. Maldovan and E. L.Thomas, Nat. Mater. **3**, 593 (2004).